

Remote Sensing and Artificial Intelligence Integration for Seabed Seagrass Habitat Mapping: A Case Study of the inner Seto Inland Sea

○Gandhi NAPITUPULU, Han Soo LEE, Vinayak Nitin BHANAGE, Yuji SAKUNO, Jae-Soon JEONG, Nobuhito MORI

(1) Introduction

Seagrass ecosystems are vital components of coastal environments, providing habitat, stabilizing sediments, and sequestering large amounts of carbon, thereby playing a key role in blue carbon storage and climate change mitigation (Park et al., 2021). Despite their ecological importance, seagrass meadows are rapidly declining worldwide due to coastal development, pollution, and climate-driven stressors, creating an urgent need for accurate, large-scale monitoring to support effective management. Satellite remote sensing, particularly using multispectral sensors such as Sentinel-2, offers a scalable and cost-effective alternative to field surveys, while recent advances in artificial intelligence (AI) have substantially improved seagrass detection accuracy (Song & Sakuno, 2023). However, mapping seagrass in optically complex coastal waters remains challenging because of water-column effects, turbidity, depth variability, and strong seasonal dynamics that limit model robustness and transferability. Focusing on the inner Seto Inland Sea (SIS), Japan, this study integrates multiband bottom-index (BI)-based water-column correction (WCC) with AI-driven classification to enhance seagrass detectability in shallow waters (<15 m), aiming to improve the reliability of satellite-based seagrass mapping for long-term blue carbon monitoring and coastal management.

(2) Data and Method

The study area is the inner SIS, Japan (Figure 1), covering shallow coastal waters (<15 m). Sentinel-2

Level-2A surface reflectance imagery (2019–2025) was processed in Google Earth Engine using Bands 2, 3, 4, and 11 at 10 m resolution; scenes with >15% cloud cover was excluded, and land and deep-water pixels were masked using the modified normalized difference water index (MNDWI). Bathymetry was derived from Japan Hydrographic Association M7000 electronic charts and resampled to 10 m. Water-column effects were reduced using depth-invariant multiband BI from band pairs BI_{2-3} , BI_{3-4} , and BI_{2-4} . Seagrass presence-absence and biomass data from Song & Sakuno (2023) and the Monitoring Sites 1000 program were used for training and validation. Classification employed seven machine learning models and two deep learning models, with performance evaluation using overall accuracy (OA) and the kappa coefficient (κ); extinction coefficient ratios (k_{ij}) temporal stability was assessed using the coefficient of variation and one-way ANOVA.

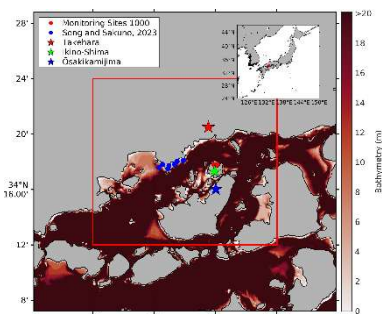


Figure 1. Study area in the inner Seto Inland Sea showing seagrass monitoring sites from the Monitoring Sites 1000 Project (red dots) and field survey points from Song and Sakuno (2023) (blue dots).

(3) Result and Discussion

The multitemporal Sentinel-2 dataset provided sufficient coverage for long-term seagrass monitoring (Figure 2), although availability was strongly constrained by seasonal cloud conditions. April and October consistently offered the highest number of cloud-free images, identifying optimal periods for optical mapping. k_{ij} exhibited low temporal variability across all band combinations, with the blue-green pair (k_{2-3}) showing the highest stability ($CV < 2\%$, $p > 0.05$), indicating reduced sensitivity to seasonal changes in turbidity and water-column properties.

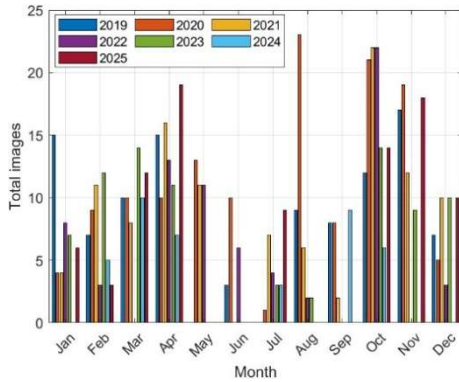


Figure 2. Monthly total of Sentinel-2 images with less than 15% cloud cover for the inner Seto Inland Sea.

Spatial patterns of the BI showed pronounced seasonal and substrate-related variability. BI_{2-3} exhibited the strongest seasonal response, with more homogeneous distributions in spring and enhanced spatial contrast in autumn, reflecting changes in water clarity and benthic reflectance, whereas BI_{2-4} and BI_{3-4} displayed broader dynamic ranges dominated by negative values due to stronger attenuation at longer wavelengths. Model evaluation confirmed that ensemble-based methods outperformed simpler classifiers, with the Random Forest (RF) model achieving the highest and most stable performance. At an optimal temporal threshold of ± 8 days, RF achieved an OA of 92.31% and a κ of 0.81, with high seagrass detection accuracy ($PA = 100\%$, $UA = 90\%$, $F1 = 0.95$). Variable importance analysis identified BI_{2-3} as the dominant predictor.

Monthly climatology revealed a clear seasonal cycle in seagrass extent (Figure 3), with minimum coverage

in winter and peak expansion from late spring to early summer, consistent with the phenology of temperate *Zostera* species (Park et al., 2021). Mapping uncertainty was higher during winter and early spring due to increased turbidity and reduced illumination, while late spring and summer provided more favorable optical conditions. The close agreement between satellite-derived patterns, field observations, and ecological expectations supports the robustness of the proposed BI–AI framework for seagrass mapping in optically complex coastal environments.

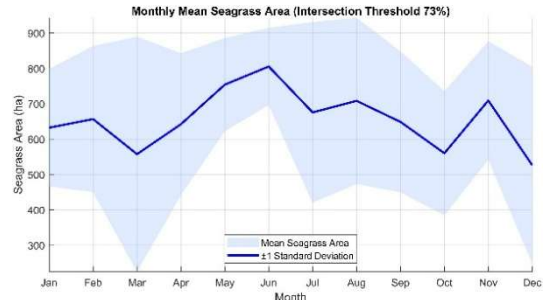


Figure 3. Monthly mean seagrass area (± 1 standard deviation) from 2019 to 2025.

(4) Conclusion

This study demonstrates that combining Sentinel-2 imagery with BI-based WCC and AI classification provides a robust approach for seagrass habitat mapping in the optically complex inner SIS. The BI_{2-3} index showed high temporal stability across seasons, while the RF classifier achieved the best performance. The proposed framework enables reliable, scalable monitoring of seagrass distribution and blue carbon assessment.

References

Song, S., & Sakuno, Y. (2023). Method for Distinguishing Sargassum and *Zostera* in the Seto Inland Sea Using Sentinel-2 Data. *Water* 2023, Vol. 15, Page 3979, 15(22), 3979.

Park, S. R., Moon, K., Kim, S. H., & Lee, K. S. (2021). Growth and photoacclimation strategies of three *Zostera* species along a vertical gradient: Implications for seagrass zonation patterns. *Frontiers in Marine Science*, 8, 594779.